Püvi, Verner; Lehtonen, Matti

Evaluating distribution network optimal structure with respect to solar hosting capacity

Published in:
Electric Power Systems Research

DOI:
10.1016/j.epsr.2022.109019

Published: 01/03/2023

Document Version
Publisher's PDF, also known as Version of record

Electric Power Systems Research 216 (2023) 109019

Contents lists available at ScienceDirect

Electric Power Systems Research

journal homepage: www.elsevier.com/locate/epsr

Evaluating distribution network optimal structure with respect to solar hosting capacity

Verner Püvi *, Matti Lehtonen

Department of Electrical Engineering and Automation, Aalto University, Maarintie 8, Espoo, 02150, Finland

ARTICLE INFO

Keywords:
Hosting capacity
Network planning
Slime mold algorithm
Voltage control

ABSTRACT

Optimal design of distribution networks has become an important topic for analysis due to the growing share of photovoltaics (PV). Low and medium voltage networks should undergo structural changes to accommodate widespread PV generation and optimal operation. In this paper, the impact of the network structure on the solar hosting capacity (HC) is analyzed with respect to the role of low and medium voltage networks in power delivery. A given set of load nodes is simulated with multiple feeding substations and varying peak power and number of PV plants. The slime mold algorithm is utilized for numerous topology generations and measured load time series represent regions ranging from rural to urban. The results reveal that networks should go through significant structural changes to cope with larger PV generation and even more so to increase the HC. On the other hand, voltage control measures, such as on-load tap changers, PV reactive power control and curtailment, provide a competitive solution to varying size of distribution networks in hosting solar power. Finally, the analysis in this study provides evidence to a possible need in the change of residential PV policies in order to sustain the current pace of adopting PV plants in Finland.

1. Introduction

Power system decarbonization has been extensively discussed in recent decades, and solar power generation by photovoltaic (PV) panels have gained considerable interest in reaching higher levels of renewable generation in the future. However, that trend place power systems into an uneasy position due to networks optimized for centralized generation and unidirectional power flow. This creates a space for study on the impact of future PV generation on the structure of current networks. Moreover, how the PV hosting capacity (HC) follows the structural changes under expected PV generation is a topic of current discussion.

Numerous works have been analyzing PV generation impact on distribution networks and considerable body of that pertains to power quality. Authors of [1] modeled centralized and distributed PV generation and observed rising power quality issues, such as voltage fluctuations and flicker. Unequally distributed PV plants cause severe deviation from nominal parameters and require network reinforcement. Likewise, voltage rise and flicker were analyzed in [2]. The loadability of networks with single- and three-phase PV plants was analyzed in [3]. The study showed that equal distribution of PV generation increases network loadability and, in addition, reactive power injection improves the loadability of networks. Authors of [4] studied voltage stability increase due to growing PV generation. Similarly, PV generation impact on voltage sags was assessed in [5]. PV generation was shown to reduce the frequency of sags due to relieved feeder loading. On the other hand, the increase of the duration of the sags was observed. An extensive review of PV impact on power quality was presented in [6]. Power quality indices, such as voltage magnitude and frequency were reviewed. The study once again emphasized serious implications on the stability and reliability of power systems caused by widespread PV adoption. Transformer (TF) power balance and capacity is analyzed with respect to PV penetration in [7]. The authors claim that for long-term planning, larger transformers should be utilized due to the increasing number of PVs and coincident generation. Network reconfiguration was utilized in [8] in order to increase PV HC by decreasing Thevenin impedance at the point of common coupling with PV plants.

Another viewing angle on the topic was shown in [9], where the policy side of the PV impact was studied. The self-consumption policies in the EU were analyzed with respect to the growing PV generation. The study has highlighted a risk of over-subsidizing PV plants, which will lead to unequal treatment of network customers. High PV penetration would increase network operation costs and further reinforcement costs, that would be later billed from all customers, no matter if they are PV owners or not. The study conducted in [10] concluded that PV curtailment would be required to maintain healthy operation of

* Corresponding author.
E-mail address: verner.puvi@aalto.fi (V. Püvi).

https://doi.org/10.1016/j.epsr.2022.109019
Received 26 January 2022; Received in revised form 13 July 2022; Accepted 20 November 2022
Available online 1 December 2022

networks, that would in turn pose an additional cost for PV owners. Consequently, investment plans can be hindered by the PV plants that are installed later down the road.

While many works focus on PV impact on power quality and policies, the impact on the network structure remains mostly unstudied. Due to the high cost of the reconstruction of distribution networks, network structures are in a locked-in state, and studies have been conducted on operational optimization, network reinforcement and expansion of current networks. On the other hand, a greenfield network design targeting maximized HC has been neglected. Knowledge of an optimal network structure in the presence of high PV generation could portray future networks, and thus help the construction of networks in developing countries. New topologies must be generated and, therefore, a network planning procedures are employed in greenfield network design.

Network planning was addressed in [11] by presenting a comprehensive MV/LV design. The node decomposition into LV distribution networks was based on k-means clustering, coupled with minimum spanning tree (MST) topology generation — a classical approach that laid a path for many other works, such as a greenfield planning solution in [12]. The cost function comprises both MV and LV networks, and distributed generation plants at candidate locations. The LV nodes are clustered by k-means clustering into load blocks that are allocated to a single substation. The feeder routing, however, relies on the MST. Results indicate, that in the presence of distributed generation, optimization of both voltage levels is beneficial. A MV/LV network planning method was presented in [13] utilizing the imperialist competitive algorithm to optimize the location of HV substation and MV feeder topology in one formulation. However, the authors fixed the location of MV/LV substations, significantly narrowing the search space for the algorithm. Moreover, the topology generation of LV networks is absent in the work. LV load nodes are connected to the closest MV/LV substation via straight connection, i.e. the star topology. A similar approach was showcased in [14], where local generation was under consideration. PV and other distributed generation plants were placed in predefined locations. The article analyzed the optimal number of microgrids with respect to deterministic and probabilistic planning while the number of local generation units remained unchanged in the analysis. A HV/MV network expansion planning algorithm was presented in [15]. The problem was formulated as mixed-integer non-linear programming and solved by the genetic algorithm with a chance constrained formulation accommodating uncertain renewable generation. Nevertheless, only one relatively small network was demonstrated with the topology consisted of predefined connections and two candidate locations for substations. Authors in [16] presented a MV/LV distribution network planning utilizing biogeography based optimization algorithm. The nodes were interconnected by predefined topologies. Similarly, the loads were divided into LV networks in [17], however each constitute the star topology. Both of the works present different number of substations for a given planning area and reveal the optimal sizes of LV networks and MV/LV network ratio. Nevertheless, both of works did not include local generation, nor included price comparison of the voltage control.

Voltage control strategies have been verified by other works conducting experimental tests using the real time digital simulators (RTDS). The authors of [18] have shown that a coordinated voltage control consisting of OLTC and RPC can be effective in increasing distributed generation hosing capacity. The correct operation of the coordinated voltage control was then verified by the RTDS. In [19] a multi-agent based voltage control was presented to increase the hosting capacity. The work investigated the communication bottlenecks that can hinder effective operation of RPC and active power curtailment, and thus the increase of the hosting capacity. A co-simulation of software- and hardware-in-the-loop is presented in [20] to evaluate the efficiency of RPC and active power curtailment of a large PV plant, and demonstrate the feasibility on deploying a transactive energy system. The study highlighted the net benefit of RPC, while the added curtailment would most likely increase the costs.

The primary purpose of this article is to analyze an optimal network structure with respect to increasing PV generation. Furthermore, we extend the concept of the number of secondary substations to track the change of HC that goes along with the structural modification. A given set of load nodes is divided into growing number of LV substations to analyze the change in cost and HC. Varying the number of LV substations entails the number of loads served by one substation and, consequently, the split of LV and MV network in the electrical power supply chain. Network size is compared to voltage control measures as one of the ways to increase HC. Time series reduction is applied to reduce the dimension of the measured load profiles to achieve acceptable balance of computation time and resistive loss estimation accuracy. Network topologies are generated by the slime mold algorithm, as a fast tool to construct a radial network while avoiding the disadvantage of the greedy approach. The cost function is formulated as the sum of cable and transformer costs of LV and MV networks. The contribution of the current work consist of tackling three challenges facing increasing PV generation.

- Analyze optimal network size of MV versus LV networks for high PV penetration and what effect has the size on the PV HC. Compare the technical and economical HC with respect to network size. Moreover, compare the PV generation and load of same peak power with respect to the change in optimal network size.
- Evaluate cost efficiency of voltage control measures such as transformers with on-load tap changers (OLTC), reactive power control of PV plants (RPC) and PV curtailment, and compare these measures to the varying network size. Whether smaller or bigger LV network is a competitive alternative for any of the PV HC increasing measures.
- Analyze the expansion of local PV generation and HC from both customers' and distribution system operator's (DSO) perspective, showing that there is a large gap between the DSO optimum of HC and the possible customer needs. Compare the current pace of PV adoption with the HC, and how it matches with the long-term perspective of accommodating PV plants.

The rest of the paper is structured as follows. Each segment of the methodology is described in Section 2. Section 3 presents the results of the analysis, followed by the conclusion in Section 4.

2. Methodology

This section further elaborates the methodology developed for the analysis. The cost function of the networks and network formation in terms of three different regions is described. After the load types are set, the dimension of customer load and PV generation power profiles are reduced by hierarchical clustering. In the next step, the slime mold algorithm is utilized to create the topology of numerous MV and LV networks. Finally, the static parameters of networks are calculated and resistive losses estimated.

2.1. Network cost

The objective function is formulated as the cost of MV and LV networks, consisting of investment and resistive loss costs of cables and transformers, as shown in Eq. (1).

$$c = c^{CB} + c^{TF} + c^{MV,CB} \tag{1}$$

$$c^{CB} = \kappa \sum_{ij} c^c L_{ij} D_{ij} + \kappa \epsilon \sum_{ijt} \tau_t c^e r L_{ij} 3 I_{ij,t}^2 \qquad (i,j) \in \omega^{LV}, t \in T \tag{2}$$

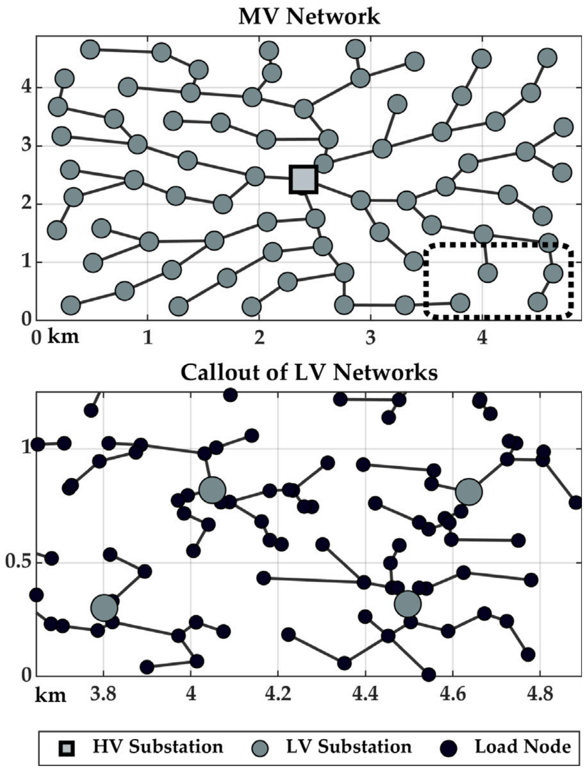

Fig. 1. Topology of MV and LV networks of suburb region.

$$c^{TF} = \kappa c^t n^{TF} + \kappa\varepsilon \left[\sum_t \tau_t c^e P^0 n^{TF} + \sum_t \tau_t c^e P^{Cu} \left(\frac{P_t^{TF}}{S^{TF}} \right)^2 \right] \quad t \in T \tag{3}$$

$$c^{MV,CB} = c^{CB} \quad (i,j) \in \omega^{MV}, t \in T \tag{4}$$

The left term of Eq. (2) entails the investment cost of the line ij, where c^c is cable cost, L_{ij} length of the line and D_{ij} is adjacency matrix. The right term is loss costs, where c^e is energy losses cost, r cable resistance and $I_{ij,t}$ is the current in line ij at time instant t. τ_t is the duration of the time instant t from the set of reduced power profile hours T. The transformer cost is formulated in Eq. (3) as a sum of investment cost, no-load cost and load costs. c^t is the cost of a single transformer and n^{TF} is the number of transformers, P^0 and P^{Cu} are TF no-load and load loss ratings, P_t^{TF} is transformer power at t, and S^{TF} is TF capacity. Eq. (4) calculates cable cost of MV network, and follows Eq. (2), except for the nodes defined over set ω^{MV}. The set of MV nodes ω^{MV} consist of one HV substation and varying number of LV substations. On the other hand, the set of LV nodes ω^{LV} consist of LV substations and the fixed number of load nodes. The annualized costs are obtained by multiplying total costs by the lifetime factor κ and the annuity factor ε, calculation of which is described in Appendix A.

2.2. Case networks

Three regions of typical network types in Finland are considered in this analysis. The regions represent rural, suburban and urban networks, each having unique customer density, customer types and network components. The density of each region is based on the survey presented in [21]. The networks, however, had fixed sizes and, for the purpose of the current analysis the network span is taken to extrapolate over a larger number of nodes. Load nodes are placed in an uniformly random order, covering up a square plane of size $d \times d$, which is based on node density ρ, as shown in Eq. (5). The number of load nodes for

Table 1
Load parameters per region [21].

	Rural	Suburb	Urban
Node density ρ (m/node)	$1200/\sqrt{8}$	$400/\sqrt{10}$	$200/\sqrt{5}$
Customer per Node	1	4	60
Storage electric heated (%)	5.9	7.6	0.5
Non-electric heated (%)	52.9	52.5	95.3
Direct electric heated (%)	41.2	39.9	4.2

current study is n^{load}=1500, which is in the same range as the largest case studies found in the literature review, e.g. [2,12,17]. Fig. 1 depicts a network solution of suburb region.

$$d = \sqrt{n^{load}} \cdot \rho \tag{5}$$

In Finland, the larger chunk of household electricity consumption comprise of heating. Three distinct heating types can be distinguished by their load profile: storage electric heating, non-electric heating and direct electric heating. The load profiles employed in this analysis were acquired during the measurement campaign in the capital region of Finland. The heating type distribution among the regions and the node densities are presented in Table 1. All customers within one node are assigned the same load type. For the sake of simplicity of the network formation process, a single cable and transformer size is considered for each region [21].

2.3. Network topology by the slime mold algorithm

In this study, the slime mold algorithm is used to form a network topology for both MV and LV networks. The algorithm is based on the behavior of a slime mold organism, *Physarum polycephalum*, and its behavior in connecting several food pieces into one nutrient transporting infrastructure. Over time, the food connecting tubes of the slime approach the shortest paths acquiring the highest transportation efficiency. However, by relaxing input parameters of the mathematical formulation of the algorithm, the topology can avoid the disadvantage of a greedy approach of the MST, and have shorter connections to the source node. An in-depth study of the slime mold algorithm conducted in [22] showed that if resistive losses are considered in the cost function along with the line length, then a slight relaxation from the MST can lead to a more optimal distribution network topology. Despite the fact that the algorithm does not require any candidate node connections, the computation burden remains low, which suits the repetitive generation of numerous networks.

Let the flux F_{ij} between nodes ij be pushed by the difference of the pressure p through a line with length L_{ij} and conductivity D_{ij}, as in Eq. (6).

$$F_{ij} = \frac{D_{ij}}{L_{ij}} \left(p_i - p_j \right) \tag{6}$$

$$\sum_j F_{ij} = \begin{cases} n^N F^0 & \text{, if } i = \text{substation} \\ -F^0 & \text{, if } i = \text{load} \end{cases} \tag{7}$$

$$D_{ij}^{k+1} = D_{ij}^k + \left| F_{ij}^k \right|^{\mu} - \gamma D_{ij}^k \tag{8}$$

Then, the flux conservation is depicted in Eq. (7), where load nodes have a flux demand of $F^0 = 0.2$ as in [22], and substation node is feeding the network with amount of flux equivalent to the number of load nodes simulated n^N. The algorithm is initialized with the adjacency matrix D_{ij} with every of its element has the conductivity value of one, i.e. every node is connected to every other node. Over the course of the iterative process, connections without flux will gradually decay as imposed by the difference Eq. (8). The pressure of each node is updated by solving the system of linear equations formed by Eq. (6). What remains is a spanning tree, that has a source node connected to every other sink node. By adjusting the input parameters μ and γ, topologies such as MST, a star network and numerous variations in between the two can be reached. The output of the algorithm is a symmetrical adjacency matrix where every node has at least one connection in upper (and lower) triangular, and the total number of connections is equal to one less than the total number of simulated nodes.

To prevent feeder load exceeding cable capacity, the customers around LV substations are divided into sectors as suggested in [22]. The number of sectors is the smallest number that satisfies the cable ampacity criterion. The load nodes are sectored by the k-means++ algorithm, that clusters nodes by their angle, measured from the feeding substation. The number of sectors starts at one and is incremented until cable ampacity requirement is met. The sectors resemble pie slices centered around an LV substation.

Similarly to LV networks, the topology of the MV network is generated by the slime mold algorithm with one cable size served as a connection type. During the topology generation only the LV substations with one HV substation, located in the middle of the plane, are considered, while the load nodes are neglected. The load of each substation incorporates the sum of the underlying load nodes and the voltage drop of the MV network side is then passed to LV network load flow calculations as an initial voltage level.

2.4. Dimensionality reduction of time series

The objective of the current analysis is to estimate resistive losses costs over a year long operation of a network. A one year long power profiles are considered for losses calculation, with one hour resolution which yields the power profiles with 8760 steps. Such resolution grants good estimation, but requires significant amount of repetitive load flow calculations. To reduce the dimensionality of the profiles, a hierarchical agglomerative clustering is used. The number of time steps can be reduced to any desired value such that the computation burden will fall significantly, while retaining acceptable level of losses approximation.

Hierarchical clustering based on Ward's minimum variance criterion finds the dissimilarity between contiguous clusters and merges the two together. In our case the algorithm starts with 8760 clusters, where each cluster represents a single hour value. The operation continues until the number of clusters reach the desired value of time steps, which in current analysis is set to one fifth of a year, that is 1752 time steps. The clustering is conducted on an initial variable that represents a two-column array, with total system load and PV generation for left and right column respectively, as follows $X_t = (PD_t^{sys}; PG_t^{sys})$, where power is the sum over all nodes $PD_t^{sys} = \sum_i PD_{i,t}$ and $PG_t^{sys} = \sum_i PG_{i,t}$. The step-by-step clustering method follows the guidelines of [23] and is described below.

1. Calculate the dissimilarity index according to Ward's criterion of every pair of contiguous clusters as shown in Eq. (9).

$$d(X_t, X_k) = \frac{2\tau_t \tau_k}{\tau_t + \tau_k} \|\bar{X}_t - \bar{X}_k\|^2 \tag{9}$$

where τ_t denotes the length of a cluster and $\bar{X}_t$ a medoid of a cluster.
2. According to the dissimilarity index, find the two contiguous clusters with the smallest dissimilarity.
3. Merge the two clusters. A single medoid $\bar{X}_t$ of a newly formed cluster is found from the set of the power profiles of the initial variable X_t. The medoid is a data point from a given set of points that is the closest to the centroid of that set [24]. The duration of the new cluster τ_t is a sum of the durations of the two merged clusters.
4. If the length of the time profile has reached the desired value, then move to the next step. Else, return to step 1.
5. The final two-column array is extrapolated from a system level to a node level power profiles $PD_{i,t}$ and $PG_{i,t}$, and is accompanied with the duration matrix τ_t.

2.5. Voltage control

In the current study, three voltage control measures are applied to increase the hosting capacity of the networks and evaluate their cost efficiency. Moreover, the comparison includes altered network sizes by changing the number of substations. First, LV transformers are replaced with counterparts equipped with on-load tap changers. The tap range is ±4%, while the cost of OLTC transformer is three times of the cost of a standard transformer. In case of voltage rise reaching upper constraint, the tap is set to −4% to lower the voltage and to provide larger margin for PV generation. A depreciation cost is followed after every tap switch and accumulates into a maintenance cost over the lifespan of a transformer. In this study, the maintenance cost caused by the switching is linearly dependent on the number of switching operations and is formulated as shown in [25] in Eq. (10).

$$c^{OLTC} = c^{main} \frac{n^{tap}}{N^{OLTC}} \tag{10}$$

The maintenance cost of an OLTC transformer c^{main} is 20% of the investment cost, n^{tap} is the number of tap operations of a single transformer and N^{OLTC} is the maximum number of tap operations without maintenance. As compared to the reference [25], in the current study two tap operations are taken into account after the tap is set from 0% to ±4%. Also, the number of maintenance-free operations of 700,000 is also modified by the ratio of the number of steps of the transformers considered in the two works 5/19. On top of that, N^{OLTC} is divided by 5 due to the reduced time series and furthermore divided by 6 to convert the 10-min to 1-h time resolution. Secondly, reactive power control is applied to all PV plants in an LV network if any of the nodes violate the upper voltage limit. The current study employs a constant power factor of 0.9 for the PV RPC. Such an approach gives fast evaluation of the RPC impact on the voltage, while providing the highest possible HC value that can be reached by the reactive power compensation. The reactive power is reserved from the nominal power of PV plants. If voltage violation will occur, the output power of a PV plant will split in between active and reactive power, thus lowering the active power output. The cost of the reduced active power output is then accounted with the cost of the curtailed power. Lastly, PV curtailment is applied on PV plants if voltage rise occur. Only violating PV plants are curtailed during required hours, unless TF node has voltage violation. In that case all PVs in the network are curtailed. The curtailment rate is 10% of the PV peak power, while the cost of the curtailed power is c^{curt}=0.01 €/kWh [26] and cost of energy loss is c^{e}=0.05 €/kWh [22].

2.6. Proposed framework

The proposed solution framework is an exhaustive calculation of network state with respect to varying number of substations, PV power and number of PV plants. Intermediate steps in between choosing a region and final recording of the violations are explained in Fig. 2. First, the given set of load nodes is divided into n number of networks, each supplied by a single TF. The partition is conducted by the MATLAB k-means++ function based on the node locations on an Euclidean xy-plane. The TF is situated at the centroid of the cluster, and is moved 10 m towards the center of the plane if it falls into same location as any other load nodes. The clustering is repeated 1000 times to reach a better cluster distribution. After the nodes are partitioned, the slime mold algorithm is utilized to generate LV topology for each network and MV topology to tie LV substations with the HV substation in the middle of the plane. Next, the dimension of the power profiles are reduced from 8760 to 1752 h with hierarchical agglomerative clustering. Finally, the load flow is conducted to evaluate the voltage and ampacity limits in the networks, followed by the evaluation of the OLTC, RPC and PV curtailment cases. Newton–Raphson-based single-phase AC load flow is utilized to calculate voltage and current levels in the system with convergence precision of the method of 1%. The feasibility of

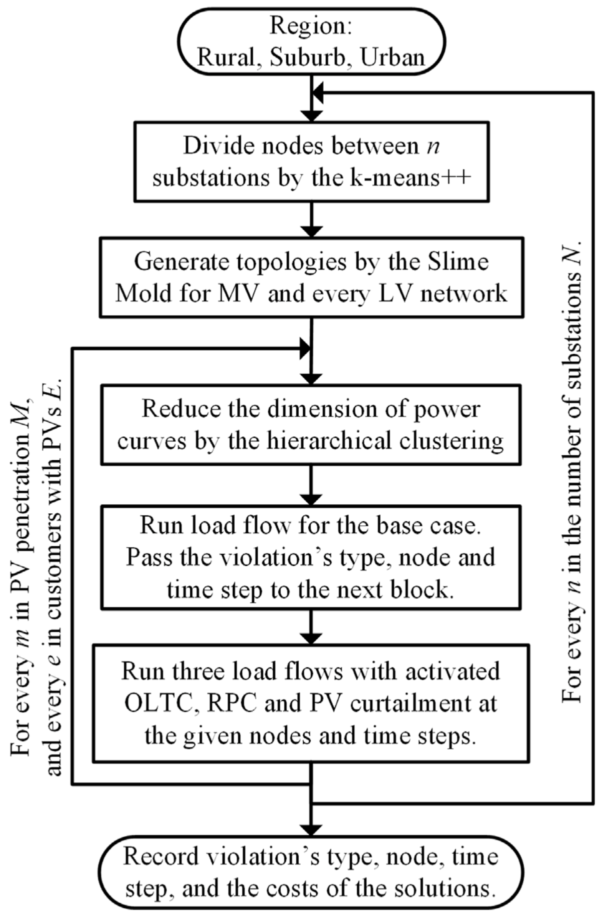

Fig. 2. Flowchart of the proposed framework.

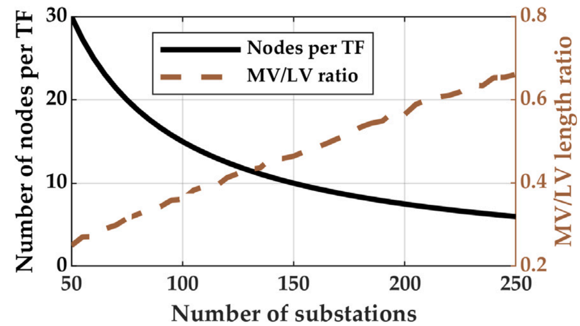

Fig. 3. Translation of the number of secondary substations (transformers) to number of nodes per substation and MV/LV network length ratio.

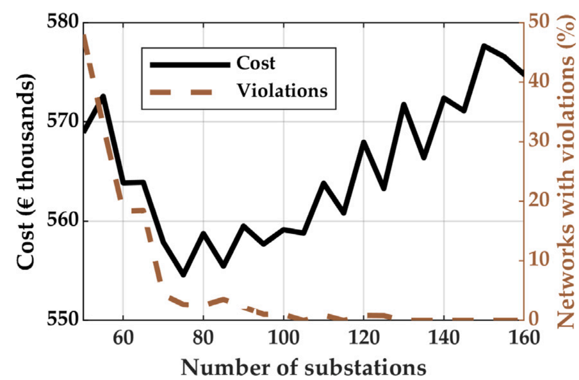

Fig. 4. Cost and the number of violations dependency on the number of substations in subrub region for the base case.

networks is evaluated based on four criteria: voltage drop, voltage rise, cable ampacity and transformer capacity. Acceptable voltage deviation from the nominal voltage is ±5%, while the LV network component capacities are listed in Tables B.8 and B.10, and the MV network cables in Table B.9 in Appendix B.

The procedure described above is repeated over the three sets. For every $m \in M = \{0, 50, 60, 70, \dots, 310\}$ which is a set of PV penetration levels measured as a share of a peak load. PV output power is incremented in steps as assigned in M. The PV generation profile employed in current study is a modeled theoretical maximum PV generation in the capital region. PV peak powers are scaled to customer ratios based on their maximum load. Such assumption is based on the work published in [27], where the authors showcased the benefit of matching the PV plant size to the load of a household. Current study believes in customers awareness and will to maximize the profits of the PV ownership, and thus assumes the PV plant dependency on the load size. For every $e \in E = \{0, 5, 10, \dots, 100\}$ which is a set of percentage of customers equipped with PV plants. PV plants are distributed among the customers with linear interpolation to equally divide PV plants over the simulated set of nodes. Such variable mimics various PV adoption scenarios that could be reduced to the number of PV plants e.g. the PV acceptance rate. As highlighted in the PV social acceptance study in [28], the citizens of Finland are environmentally concerned, and in conjunction with effective support policy and adequate information, the PV acceptance rate could be greatly increased. In recent years the household/individual PV installations is a major and fastest-growing segment in Finland, and is expected to reach 150 thousand PV plants by the year 2024. Based on that, current study assumes the acceptance rate is higher than the HC. Lastly, for every $n \in N = \{50, 55, 60, \dots, 250\}$ which is a set of number of substations. In the current work, the term *number of substations* is utilized to reflect the structure of networks. Due to the clear meaning and linear property of the metric, the term is used throughout the current analysis. However, the number of substations is strongly related to the actual size and number of nodes in the network. To allow compatibility with other works, Fig. 3 shows the translation of the metric to other indices, such as the average number of nodes served by one secondary substation and ratio of the MV/LV network lengths.

3. Results

In this section, the results of the analysis and major observations are presented. The simulation is carried out in MATLAB R2021a.

3.1. Optimal number of substations

First, finding the optimal number of substations is described, as it is used in results analysis of forthcoming sections. The optimal number of substations is a feasible solution with the lowest cost. Network feasibility is evaluated based on the four criteria outlined in Section 2.1, and are shown as a percentage of networks falling short on meeting the requirements. Similarly to [21], the 5% threshold is employed to eliminate outlier solutions and include the tolerance margin. If more than 5% of the networks on the plane have power quality violations, the whole solution is considered infeasible. The total network cost curve and share of networks with violations of the suburb network can be seen on Fig. 4. The same evaluation is applied to rural and urban regions and the optimal number of substations of all the regions are summarized in Table 2. Note that the optimal number of substations is denoted as "Optim." for the rest of the paper.

Table 2
Optimal number of substations (transformers) in each region for the base case.

	Rural	Suburb	Urban
Optim.	185	75	160

Table 3
Comparison of the optimal number of substations at equal load and PV power peaks.

	Rural	Suburb	Urban
No PV	170	70	105
With PV	235	85	115

3.2. Technical and economical hosting capacity

Building from the research in [29], two distinguishable types of HC are advanced next. The technical HC, that quantifies maximum allowable PV penetration constrained by power quality requirements and network component limits. Secondly, the economical HC, which is constrained by the losses of the network. Due to the U-shaped losses curve dependency on PV penetration, the losses drop when PVs are firstly introduced to the network. If PV generation is increased further, the losses start to rise again after passing the bottom of the U-curve. To avoid excessive loss costs, a DSO can set a limit at the point where the network losses equal the base case without PV generation, and current paper considers that point as the economical HC.

As Fig. 5 demonstrates, network size has strong impact on technical HC. Smaller LV networks are directly correlated with higher HC (with respect to peak load). On the other hand, economical HC demonstrates the opposite correlation. Larger and less efficient networks dispose towards higher economical HC levels. Larger resistive losses before PV adoption will grant higher margin for the losses caused by PV generation. Though, the magnitude of the benefit is low at the economical HC, and urban networks are even less responsive to the network size.

3.3. Coincident peaks

A comparison of two networks is shown next to demonstrate the effect of coincident peaks of PV generation and load. First, a feasible network structure with the smallest number of substations is found, while the cost is neglected. Such structure reflects the suitable network sizes for the case without any PV plants in the network. Then, the first feasible network is found for the case with PV generation with such output power, that the net power equals the peak of the load. The PV peak power is higher than the actual value of the load to compensate the load during the sunshine hours, equalizing the net power flow of the peaks.

A network size comparison reveals the issue of highly coincident PV generation peaks. Table 3 shows that an inclusion of PV generation requires smaller LV networks to compensate larger power flows. Despite the same net peak powers, the solar generation highly coincident at noon hours and strains the networks at higher extent than the load. Fig. 6 supports the observations as it depicts the rise of the coincidence factor as the PVs are introduced. The coincidence factor is formed by the peaks of the load, and remains unchanged until the solar generation peaks start to rise. Once the net peak of the solar generation is equal to the peak of the load, the coincidence factor reaches values close to one.

3.4. Voltage control against network size

The network sizes are compared to commonly accepted voltage control methods: OLTC, RPC of PV plants and PV curtailment. Fig. 7 depicts the effect of the aforementioned methods with the optimal number of substations deviated along the set N in three positive and three negative groups. Each group contains three values ± 5, 10, 15,

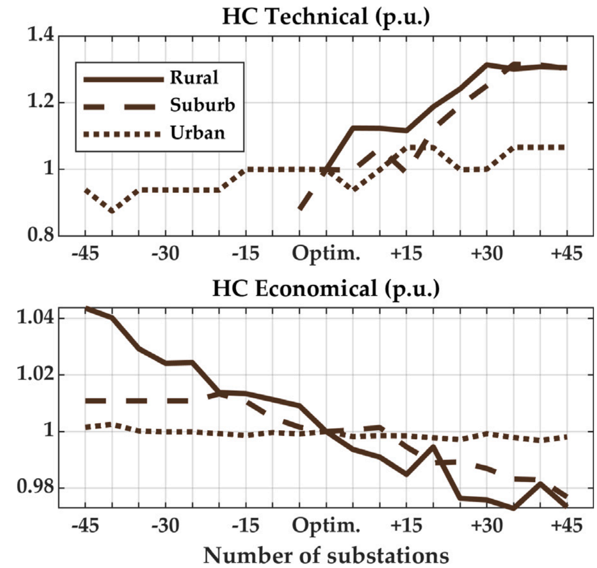

Fig. 5. Technical and economical hosting capacities (wrt. peak load) dependency on the number of substations.

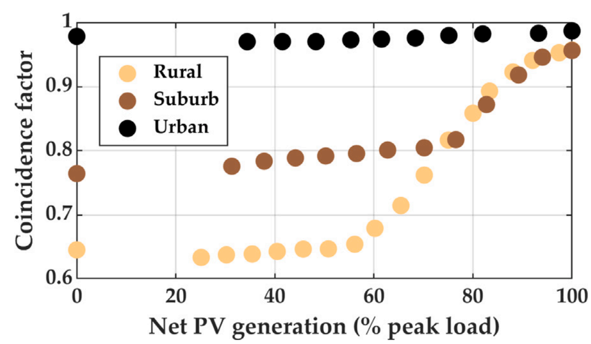

Fig. 6. Coincidence factor against the net PV power as a share of peak load, average over all LV networks.

± 20, 25, 30 and ± 35, 40, 45 substations. The figure shows the average values of each triplet, where they are denoted by $+(-)$, $++(--)$ and $+++(---)$ respectively. As indicated in the upper most subplot, the rural network would benefit of OLTC the most, despite the higher cost. Suburban networks are the middle ground, where both voltage rise and capacity constraint limit the HC. All the methods increase HC, while the smaller LV networks give comparable increase of HC as OLTC transformers and RPC. Urban networks undergo capacity constraints, thus splitting loads between more substations, PV curtailment and RPC provide the best increase in HC, while OLTC remains futile.

3.5. Highest PV injected power

The generally accepted customer connection power in Finland is 3×25 A, that is approx. 17 kW. The connection size is defined in [30] as the amount of electricity to be distributed through the connection. The connection power is granted by DSOs and every customer has the right to consume that amount of power. If not otherwise noted, customers are allowed to inject to the network as much power as the connection capacity accounts for. If the technical limits of the distribution network will limit the PV penetration before the 17 kW connection limit, the customers have the moral right to demand the DSO to reinforce the network to be capable to export as much as they import from the network with no additional cost to the customer.

Fig. 8 shows that, at the point of network optimal HC, the average injected PV power of the customers in all the regions is well below

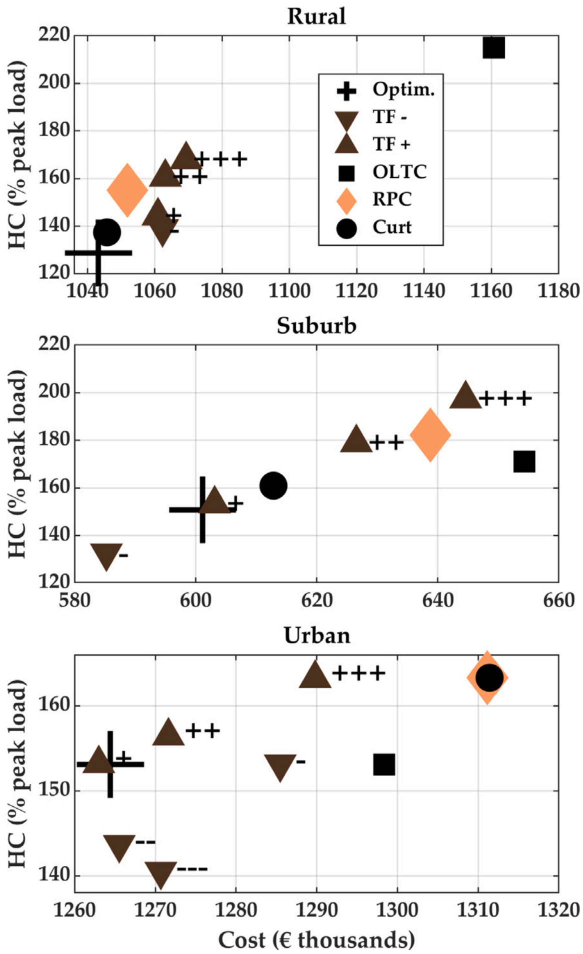

Fig. 7. Voltage control in comparison to optimal, smaller (TF−) or larger (TF+) number of substation.

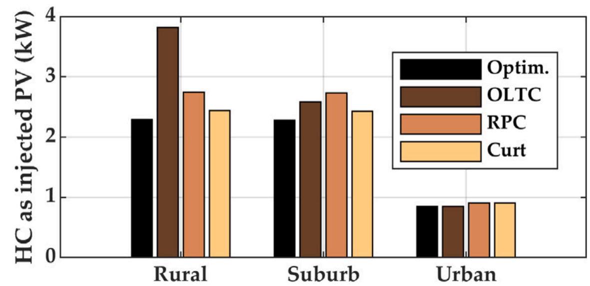

Fig. 8. Hosting capacity as average PV injected power per customer.

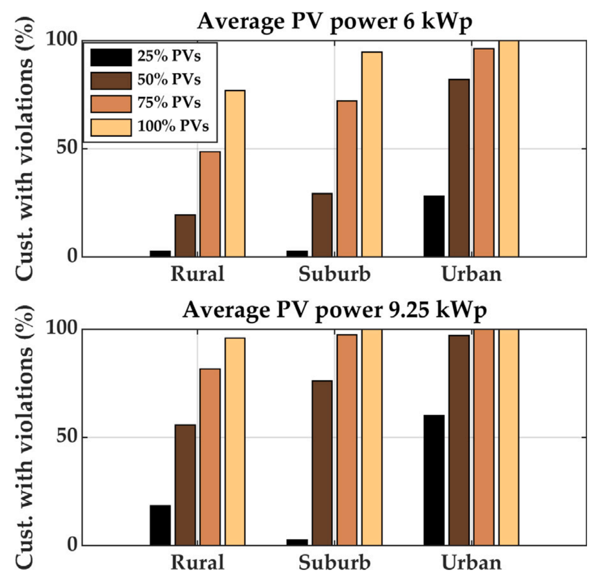

Fig. 9. Customers with power quality violation at four different shares of customers having either a 6 or 9.25 kWp PV plants.

the connection power limit, typically only 15%–20% of the connection size. Rural and suburb region networks can withstand PV power of around 2.5 kWp. RPC and curtailment can rise the ceiling up until 2.75 kWp, and OLTC even higher. The urban region has the lowest withstand power of ca. 1 kWp, and voltage control can hardly help. However, the urban region has the largest number of customers per node and all the customers have PV plants in the results under discussion. The hosting capacity dependency on the number of PV plants is analyzed in the next sections.

3.6. Current pace of PV adoption

In this section, the current pace of adopting PV plants is analyzed with respect to the number of customers with PV plants. Research published in [27] have analyzed the building stock of Helsinki metropolitan area and concluded that an average PV peak power for residential customers having own generation is 6 kWp. Moreover, author of [31] revealed the average PV installation peak of one of the DSOs in Finland to be 9.25 kWp. Given the two numbers, the PV penetration is analyzed with respect to the number of customers with PV plants in the following section.

The highest feasible share of customers equipped with PV plants is shown in Table 4. Up to 25% of customers in rural region can host average PV plants of 6 kWp, while the 9.25 kWp will decrease the share until 10%. Voltage control measures can twofold the number of customers with PVs. The suburb region demonstrates a similar performance. Nevertheless, the voltage control measures are less effective

Table 4
Maximum feasible share of customers (%) with PV plants if average PV plant sizes are 6 and 9.25 kWp.

Mean PV	Rural	Suburb	Urban
6.00 kWp	25	35	10
+ OLTC	60	40	10
+ RPC	30	45	15
+ Curt.	30	35	15
9.25 kWp	10	25	5
+ OLTC	30	25	5
+ RPC	15	25	10
+ Curt.	15	25	10

in increasing the share of prosumers as compared to rural networks. Lastly, the urban region shows the lowest share of customers and the voltage control has negligible effect on the outcome. However, the small share of customers can be explained by the vast difference in the number of customers per node.

The number of PV owners is expected to dramatically increase in the future, and therefore Fig. 9 depicts the number of power quality violations at high share of customers with PVs. Due to the high number of customers, the urban region networks will be the first who will reach the HC limit if the current pace of PV installations will continue. In the rural and suburb regions up until one quarter of customers can install PV plants at current rate without any restrictions. Still, high numbers of currently installed PV plants are infeasible with current networks.

Table 5
Optimal number of substations at the PV HC point at average PV plant sizes of 6 and 9.25 kWp.

Mean PV	Rural	Suburb	Urban
No PV	185	75	160
6.00 kWp	245	105	165
9.25 kWp	250	105	165

3.7. Optimal network size at current pace of PV adoption

Contrary to the previous section, an optimal number of substations is analyzed below. Table 5 outlines the trend of optimal network sizes. At current rate of PV adoption of average 6 and 9.25 kWp PV plants, the optimal network size shifts to smaller LV networks i.e. larger number of secondary substations. The more PV plants of the current average sizes are introduced to networks, the less economically viable is the network operation. To keep costs from rising significantly in the future, the LV networks should be smaller.

4. Conclusions

The continuously growing number of PV plants requires to analyze the effect of PV generation on network structure. In this paper, three regions based on typical distribution networks in Finland with a given set of 1500 load nodes were simulated at a different number of LV substations. Furthermore, a solar hosting capacity was found by increasing solar generation in two terms: PV peak power and the number of customers equipped with PV plants.

The main objective of the work is to observe how the number of LV substations changes the PV hosting capacity of the network. Technical and economical HC were compared to the growing number of substations. Larger number of substations favor technical HC, as the strain from LV network is shifted to MV side. On the other hand, smaller number of substations (larger LV networks) show higher economical HC. Larger resistive losses before PV adoption will grant larger margin for the losses caused by PV generation. Moreover, the study has shown that PV generation of the same net peak power as load, strains the networks to a higher extent.

Secondly, the varying number of substations has shown to be a valid competitor to commonly accepted voltage control. However, voltage control cost efficiency has shown to be dependent on the applied region. In the rural region, the OLTC provides by far the highest increase in HC, while RPC and curtailment takes the lead in the urban region. The suburb region combines the effects of both. Increasing the number of substations leads to higher HC in all the regions equally. However, the added cost of the substations holds the price around the same level. From another standpoint, the share of customers with PV plants can be increased up until twofold by adopting voltage control measures.

Finally, the results indicate that the network HC as injected PV power per customer is much lower than connection size across all the regions. Customers have the moral right to demand network reinforcement to be able to export as much power as they may import. On the other hand, DSOs could potentially change the policy to escape enormous network reinforcement expenses, and set separate limits for export and import in the future. Moreover, by extrapolating the average installed PV plant sizes, the current pace of installations leads to the conclusion that the average PV plants should be downsized, or customers should be restricted to connect their PV plants to the network in the future due to depleted HC.

In addition to the solar power, distribution networks will be exposed to other power sources. The method proposed in the current study has few drawbacks, such as the lack of the global optimum solution and cumbersome power dispatch modeling requires to take a next step in the problem formulation. To ensure the fairness of the network structure studies, the proposed framework will be extended in the future work to include other renewable sources and emerging electric vehicle charging in distribution networks. Therefore, for such complicated networks with numerous devices willing for controlled power exchange, the current deterministic load flow calculation will be abandoned. Instead, an optimal power flow will be adopted to find the hosting capacity in a single calculation while retaining the global optimum solution. The formulation of such task requires it to be convex, and while having reactive power included in the formulation, it should stay from being highly non linear. Moreover, the computation time should be reduced in order to simulate all the thousands networks that are generated during the network structure studies by utilizing as least integer variables as possible.

Nomenclature

Please follow Table 6.

CRediT authorship contribution statement

Verner Püvi: Methodology, Software, Formal analysis, Investigation, Writing – original draft, Visualization. **Matti Lehtonen:** Conceptualization, Validation, Resources, Data curation, Writing – review & editing, Supervision, Project administration, Funding acquisition.

Declaration of competing interest

The authors declare that they have no known competing financial interests or personal relationships that could have appeared to influence the work reported in this paper.

Data availability

The data that has been used is confidential.

Funding

This work was supported by Aalto University of Finland as a part of “SolarX” project 211763 funded by Business Finland.

Appendix A. Lifetime and annuity factors

The distribution network construction cost is paid once, in the beginning of the planning period, and this is called the investment cost. After the payment, however, the cost is returned to a creditor in annual amounts. To find the required annual transfer amount and incorporate money depreciation during the planning period T_p (network lifetime) by the interest rate p, the total cost is multiplied by the annuity factor ε (A.1). The network planning parameters for discount factor calculation are shown in Table A.7:

$$\varepsilon = b \times \frac{1}{1 - \frac{1}{(1+b)^{T_b}}} \tag{A.1}$$

Resistive loss costs, on the other hand, constitute annual losses that need to be covered every year during the planning period. Load has a tendency to grow at rate g over the load growth period T_g. The total loss costs in net present value over the planning period can be found by multiplying the first year loss costs by the lifetime factor κ (A.2). Parameters α_1 and α_2 required for lifetime factor calculation are derived in Eqs. (A.3) and (A.4). The annual payment of the loss costs is then found by multiplying the total cost by the annuity factor ε.

$$\kappa = \alpha_1 \times \frac{\alpha_1^{T_g} - 1}{\alpha_1 - 1} + \alpha_2 \times \frac{(1+g)^{2T_g}}{(1+b)^{T_g}} \times \frac{\alpha_2^{T_b - T_g} - 1}{\alpha_2 - 1} \tag{A.2}$$

Table 6
The following abbreviations and nomenclature are used in this manuscript.

	Abbreviations
DSO	Distribution system operator
HC	Hosting capacity
MST	Minimum spanning tree
OLTC	On-load tap changer
PV	Photovoltaic
RPC	Reactive power control
TF	Transformer
	Nomenclature
c	Network total cost, €
c^c	Cable cost, €/m
c^{CB}	LV cable cost, €
c^{curt}	Cost of energy curtailed, €/kWh
c^e	Cost of energy loss, €/kWh
c^{main}	Single OLTC maintenance cost, €
$c^{MV,CB}$	MV cable cost, €
c^{OLTC}	Total OLTC maintenance cost, €
c^t	Cost of a transformer, €/piece
c^{TF}	LV transformer cost, €
d	Network span, m
D_{ij}	Conductivity adjacency matrix
e	Index of share of customers with PV plants
E	Set of customers equipped with PV plants, %
F_{ij}	Flux between nodes ij
F^0	Load node flux demand
$i\ j$	Indices of nodes
$I_{ij,t}$	Current in line ij at t, A
L_{ij}	Line ij length, m
m	Index of PV power level
M	Set of PV penetration levels as peak load, %
n^N	Number of simulated load nodes
n^{load}	Total number of load nodes
N^{OLTC}	Number of maintenance-free tap operations
n^{tap}	Number of tap operations of a transformer
n^{TF}	Number of transformers
n	Index of number of substations
N	Set of number of substations simulated
p_i	Pressure at node i
P^0	Transformer no-load loss rating, W
P^{Cu}	Transformer load loss rating, W
PD_t^{sys}	Power demand of system at t, W
PG_t^{sys}	Power generation of system at t, W
$PD_{i,t}$	Power demand at node i and time t, W
$PG_{i,t}$	Power generation at node i and time t, W
P_t^{TF}	Transformer power at time t, W
r	Cable resistance, Ω/m
S^{TF}	Transformer capacity, W
$t\ k$	Indices of time instant
T	Set of reduced power profile hours
X_t	Total load and generation at t, W
γ	Tube decay rate
ε	Annuity factor
κ	Lifetime factor
μ	Flow feedback rate
ρ	Node density, m/node
τ_t	Duration of a time instant t, h
ω^{LV}	Set of low-voltage nodes
ω^{MV}	Set of medium-voltage nodes

$$\alpha_1 = \frac{(1+g)^2}{1+b} \tag{A.3}$$

$$\alpha_2 = \frac{1}{1+b} \tag{A.4}$$

Appendix B. Technical parameters

The LV cable and transformer data used in the current article are shown in Tables B.8 and B.10. The MV cable data is shown in Table B.9. The technical parameters are taken from the datasheets of manufacturers in Finland, and costs are based on data by The Energy Authority of Finland [32].

Table A.7
Discount factor parameters.

Parameter	Symbol	Value	Unit
Planning period	T_b	40	year
Load growth period	T_g	20	year
Interest rate	b	1.05	p.u.
Load growth rate	g	1.05	p.u.

Table B.8
LV cable parameters.

Region	Size (mm^2)	Ampacity I^{CB} (A)	Impedance z (Ω/km)	Cost c^c (€/m)
Rural	70	185	0.53+j0.08	32.7
Suburb	185	330	0.20+j0.08	54.3
Urban	2 × 185	2 × 330	0.10+j0.08	2 × 54.3

Table B.9
MV cable parameters.

Region	Size (mm^2)	Ampacity I^{CB} (A)	Impedance z (Ω/km)	Cost c^c (€/m)
Rural	35	210	0.89+j0.38	21.8
Suburb	55	280	0.53+j0.28	25.1
Urban	95	360	0.34+j0.27	29.1

Table B.10
Transformer parameters (0.4/20 kV).

Region	Capacity S^{TF} (kVA)	Impedance z (Ω)	No-load P^0 (W)	Load P^{Cu} (W)	Cost c^t (€)
Rural	50	0.070+j0.11	90	1100	4810
Suburb	250	0.008+j0.02	300	3250	8661
Urban	1000	0.002+j0.01	770	10 500	20 800

References

[1] M. Ebad, W.M. Grady, An approach for assessing high-penetration PV impact on distribution feeders, Electr. Power Syst. Res. 133 (2016) 347–354, http://dx.doi.org/10.1016/j.epsr.2015.12.026.

[2] F. Ferdowsi, S. Mehraeen, G.B. Upton, Assessing distribution network sensitivity to voltage rise and flicker under high penetration of behind-the-meter solar, Renew. Energy 152 (2020) 1227–1240, http://dx.doi.org/10.1016/j.renene.2019.12.124.

[3] J. Yaghoobi, M. Islam, N. Mithulananthan, Analytical approach to assess the loadability of unbalanced distribution grid with rooftop PV units, Appl. Energy 211 (2018) 358–367, http://dx.doi.org/10.1016/j.apenergy.2017.11.030.

[4] B.A. Bhatti, R. Broadwater, M. Dilek, Analyzing impact of distributed PV generation on integrated transmission & distribution system voltage stability—A graph trace analysis based approach, Energies 13 (17) (2020) 4526, http://dx.doi.org/10.3390/en13174526.

[5] J.E.R. Baptista, A.B. Rodrigues, M. da Guia da Silva, Probabilistic analysis of PV generation impacts on voltage sags in LV distribution networks considering failure rates dependent on feeder loading, IEEE Trans. Sustain. Energy 10 (3) (2019) 1342–1350, http://dx.doi.org/10.1109/TSTE.2018.2866931.

[6] O. Gandhi, D.S. Kumar, C.D. Rodríguez-Gallegos, D. Srinivasan, Review of power system impacts at high PV penetration Part I: Factors limiting PV penetration, Sol. Energy 210 (2020) 181–201, http://dx.doi.org/10.1016/j.solener.2020.06.097.

[7] S. Freitas, T. Santos, M.C. Brito, Impact of large scale PV deployment in the sizing of urban distribution transformers, Renew. Energy 119 (2018) 767–776, http://dx.doi.org/10.1016/j.renene.2017.10.096.

[8] S. Jothibasu, A. Dubey, S. Santoso, Two-stage distribution circuit design framework for high levels of photovoltaic generation, IEEE Trans. Power Syst. 34 (6) (2019) 5217–5226, http://dx.doi.org/10.1109/TPWRS.2018.2871640.

[9] C. Mateo, R. Cossent, T. Gómez, G. Prettico, P. Frías, G. Fulli, A. Meletiou, F. Postigo, Impact of solar PV self-consumption policies on distribution networks and regulatory implications, Sol. Energy 176 (2018) 62–72, http://dx.doi.org/10.1016/j.solener.2018.10.015.

[10] G. Pillai, G. Putrus, N. Pearsall, T. Georgitsioti, The effect of distribution network on the annual energy yield and economic performance of residential PV systems under high penetration, Renew. Energy 108 (2017) 144–155, http://dx.doi.org/10.1016/j.renene.2017.02.047.

[11] L. Gonzalez-Sotres, C. Mateo Domingo, A. Sanchez-Miralles, M. Alvar Miro, Large-scale MV/LV transformer substation planning considering network costs

and flexible area decomposition, IEEE Trans. Power Deliv. 28 (4) (2013) 2245–2253, http://dx.doi.org/10.1109/TPWRD.2013.2258944.
[12] R. Gholizadeh-Roshanagh, S. Najafi-Ravadanegh, S.H. Hosseinian, A framework for optimal coordinated primary-secondary planning of distribution systems considering MV distributed generation, IEEE Trans. Smart Grid 9 (2) (2018) 1408–1415, http://dx.doi.org/10.1109/TSG.2016.2590425.
[13] S.N. Ravadanegh, R. Gholizadeh-Roshanagh, On optimal multistage electric power distribution networks expansion planning, Int. J. Electr. Power Energy Syst. 54 (2014) 487–497, http://dx.doi.org/10.1016/j.ijepes.2013.07.008.
[14] S. Mojtahedzadeh, S.N. Ravadanegh, M.-R. Haghifam, Optimal multiple microgrids based forming of greenfield distribution network under uncertainty, IET Renew. Power Gener. 11 (7) (2017) 1059–1068, http://dx.doi.org/10.1049/iet-rpg.2016.0934.
[15] P. Salyani, J. Salehi, F. Samadi Gazijahani, Chance constrained simultaneous optimization of substations, feeders, renewable and non-renewable distributed generations in distribution network, Electr. Power Syst. Res. 158 (2018) 56–69, http://dx.doi.org/10.1016/j.epsr.2017.12.032.
[16] M. Yosef, M. Sayed, H.K. Youssef, Allocation and sizing of distribution transformers and feeders for optimal planning of MV/LV distribution networks using optimal integrated biogeography based optimization method, Electr. Power Syst. Res. 128 (2015) 100–112, http://dx.doi.org/10.1016/j.epsr.2015.06.022.
[17] M. Kalantari Khandani, A. Askarzadeh, Optimal MV/LV transformer allocation in distribution network for power losses reduction and cost minimization: A new multi-objective framework, Int. Trans. Electr. Energy Syst. 30 (6) (2020) http://dx.doi.org/10.1002/2050-7038.12361.
[18] A. Kulmala, A. Mutanen, A. Koto, S. Repo, P. Jarventausta, RTDS verification of a coordinated voltage control implementation for distribution networks with distributed generation, in: 2010 IEEE PES Innovative Smart Grid Technologies Conference Europe (ISGT Europe), IEEE, 2010, pp. 1–8, http://dx.doi.org/10.1109/ISGTEUROPE.2010.5638896, URL http://ieeexplore.ieee.org/document/5638896/.
[19] A. Arshad, J. Ekström, M. Lehtonen, Multi-agent based distributed voltage regulation scheme with grid-tied inverters in active distribution networks, Electr. Power Syst. Res. 160 (2018) 180–190, http://dx.doi.org/10.1016/j.epsr.2018.02.015, URL https://linkinghub.elsevier.com/retrieve/pii/S0378779618300580.
[20] M.R. Alam, M. Alam, A. Somani, R.B. Melton, W. Tushar, F. Bai, R. Yan, T.K. Saha, Evaluating the feasibility of transactive approach for voltage management using inverters of a PV plant, Appl. Energy 291 (2021) 116844, http://dx.doi.org/10.1016/j.apenergy.2021.116844, URL https://linkinghub.elsevier.com/retrieve/pii/S0306261921003391.
[21] A. Arshad, M. Lindner, M. Lehtonen, An analysis of photo-voltaic hosting capacity in finnish low voltage distribution networks, Energies 10 (11) (2017) 1702, http://dx.doi.org/10.3390/en10111702.
[22] V. Püvi, R.J. Millar, E. Saarijärvi, K. Hayami, T. Arbelot, M. Lehtonen, Slime mold inspired distribution network initial solution, Energies 13 (23) (2020) 6278, http://dx.doi.org/10.3390/en13236278.
[23] A.A. Bashir, A. Lund, M. Pourakbari-Kasmaei, M. Lehtonen, Optimizing power and heat sector coupling for the implementation of carbon-free communities, Energies 14 (7) (2021) 1911, http://dx.doi.org/10.3390/en14071911.
[24] O. Raventós, J. Bartels, Evaluation of temporal complexity reduction techniques applied to storage expansion planning in power system models, Energies 13 (4) (2020) 988, http://dx.doi.org/10.3390/en13040988.
[25] N. Efkarpidis, T. De Rybel, J. Driesen, Optimization control scheme utilizing small-scale distributed generators and OLTC distribution transformers, Sustain. Energy, Grids Netw. 8 (2016) 74–84, http://dx.doi.org/10.1016/j.segan.2016.09.002, URL https://linkinghub.elsevier.com/retrieve/pii/S2352467716300728.
[26] A.A. Bashir, M. Pourakbari-Kasmaei, J. Contreras, M. Lehtonen, A novel energy scheduling framework for reliable and economic operation of islanded and grid-connected microgrids, Electr. Power Syst. Res. 171 (2019) 85–96, http://dx.doi.org/10.1016/j.epsr.2019.02.010.
[27] J. Vimpari, S. Junnila, Estimating the diffusion of rooftop PVs: A real estate economics perspective, Energy 172 (2019) 1087–1097, http://dx.doi.org/10.1016/j.energy.2019.02.049.
[28] M.A. Hai, Rethinking the social acceptance of solar energy: Exploring "states of willingness" in Finland, Energy Res. Soc. Sci. 51 (2019) 96–106, http://dx.doi.org/10.1016/j.erss.2018.12.013, URL https://linkinghub.elsevier.com/retrieve/pii/S2214629618302718.
[29] S. Fatima, V. Püvi, A. Arshad, M. Pourakbari-Kasmaei, M. Lehtonen, Comparison of economical and technical photovoltaic hosting capacity limits in distribution networks, Energies 14 (9) (2021) 2405, http://dx.doi.org/10.3390/en14092405, URL https://www.mdpi.com/1996-1073/14/9/2405.
[30] I. Lehto, S. Naukkarinen, Terms of network connection, 2019, URL https://energia.fi/uutishuone/materiaalipankki/liittymisehdot_-_le_2019_(myos_ruotsiksi_ja_englanniksi).html#material-view.
[31] T. Sandell, Sähkön Hajautetun Pientuotannon Kehitys Jakeluverkoissa Ja Vaikutukset Verkon Käyttöön (Master's thesis), Aalto University, 2021.
[32] E. Authority, Regulation Methods in the Fourth Regulatory Period of 1 January 2016–31 December 2019 and the Fifth Regulatory Period of 1 January 2020–31 December 2023; Appendix 2, Tech. rep., Energy Authority, Helsinki, Finland, 2015.